Al-Azhar Bulletin of Science, Section D, Vol. 33, No. 2, (December) 2022, pp.145-157
http://doi.10.21608/absb.2022.130892.1178

Al-Azhar Bulletin of Science: Section D

GEOCHEMICAL EXPLORATION OF U-MO-W YOUNGER LATE-OROGENIC GRANITES, EL-URF - EL-DOB - ABU-KHARIF GEOCHEMICAL PROVINCE, SAFAGA-QENA TECTONIC DISCONTINUITY BELT, EASTERN DESERT, EGYPT

Islam M. El-Naggar [a], Mahmoud M. Hassaan [a], Taher M. Shahin [a], Sayed A. Omar [b], Ahmed E. Khalil [c]

[a] Geology Department, Faculty of Sciences, Al-Azhar University, Nasr City, Cairo, Egypt.
[b] Nuclear Materials Authority (NMA), Maadi, Cairo, Egypt.
[c] National Research Center (NRC), Dokki, Giza, Egypt.
*Corresponding author: mah_hassaan.201@azhar.edu.eg
Received: 01 Apr 2022; Revised: 25 Apr 2022; Accepted: 28 Apr 2022; Published: 01 Dec 2022

ABSTRACT

El-Urf, El-Dob and Abu-Kharif Late-Orogenic Granite bodies are located north Safaga-Qena Tectonic Discontinuity, between latitudes of 26° 37′ and 26° 50′ N, and longitudes of 33° 20′ and 33° 28′ E. These three bodies constitute a geochemical province where El-Urf granite is bearing uranium, while El-Dob and Abu-Kharif Y Gr are hosting tungsten-molybdenum and tungsten respectively. Fieldwork integrated with remote sensing techniques and geochemical studies identified controlling factors, pathfinders, and the genesis of these deposits. The rock types, structures, and alteration processes are identified. The geochemical analyses of host rocks indicate alkali, highly fractionated calc-alkaline to alkaline, within plate to volcanic arc granites. Monzo-Syeno-Alkali feldspar and ferrugenated altered samples are identified using Fe_2O_3 VS each of MgO and CaO geochemical binary relationships. The positive correlation patterns for Zr VS K and negative for Na_2O VS K_2O and Sr VS Rb are geochemical pathfinders for such Y Gr mineralized bodies. The uranium mineralization of El-Urf granite is considered related to the genesis of the El-Erediya El-Missikat uranium molybdenum porphyry deposit. The formation of these deposits involved input in large chamber magma pulses were a magmatic hydrothermal fluid in the core of hydrothermal system and convected heated rushed Mozambique oceanic water transported the ore metals in the outer alteration zone of the upper crust. A second input of magma pulses in the large chamber formed three studied granites and the heated hydrothermal rushed Mozambique oceanic water that formed in the upper crust the W- Mo and W and Cu, Zn sulfide mineralization.

Keywords: Geochemical Exploration; U-Mo-W mineralization; Geochemical pathfinders; Eastern Desert

1. INTRODUCTION

The northern part of Nubian Shield exposed in the Eastern Desert represent the Pan-African tectonism between 800 Ma and 614 Ma [1]. It is dissected by Marsa-Allam- Idfu and Safaga-Qena tectonic discontinuities into Southern, Central and Northern domains [2].

Convergence stage of the African tectonism occurred between West and East Gondwana fragments ending the closure of Mozambique Ocean along the East African-Antarctic Orogen (EAAO) [3&4]. The whole belt acquired an emplacement of a Cordilleran character subduction-related calc-alkaline Older Syn-orogenic (O Gr) and Younger late-orogenic Granites (Y Gr), and mantle-derived mafic-ultramafic intrusions [5]. Its rock unites are chiefly Neoproterozoic accreted ophiolites, island arc rocks, Older Syn-orogenic granites (O. Gr.), Dokhan volcanics and Y Gr . Large masses of alkaline to per alkaline granites such as Gebel El-Zeit, Gattar [6&7] and Abu-Kharif riebeckite granite [8&9] were formed during the late-to post-orogenic stages.

The Nubian shield in its early stage consisted of a passive continental margin and a backarc environment. However, the Late Proterozoic igneous and metamorphic basement complexes of the Nubian Shield in Eastern Desert of Egypt comprise three domains; southern (from the Egyptian border line to Idfu-Marsa Alam road), central (between the Idfu-Marsa Alam and Qena-Safaga asphaltic roads) and northern (north Qena-Safaga road) showing three different stages. These three domains are separated by Idfu-Marsa Alam and Qena-Safaga tectonic discontinuities [2]. The southern and central domains are distinguished by ophiolitic, island arc, calc-alkaline volcanic, volcano-sedimentary rocks and metagabbro. This stage is ended by Atallha shear zone northwest and the Meatique Group ophiolitic sequence northeast Quseir-Qift road. The cordilleran stage is represented by Older Syn-Orogenic and Younger Late-Orogenic Granites; tonalite-granodiorite, and Monzo-, syeno-, and alkali feldspar granite respectively.

The units of the basement complex were interpreted and grouped by [7] into the following litho-tectonic units that developed mainly during the Pan-African orogeny as follows: Pre-Pan African genisses and migmatites; ophiolites (serpentinite, and associated talc-quartz carbonates, metagabbro and plagiogranites); island arc (metavolcanics, volcaniclastics, metasediments and calc-alkaline plutonism metagabbro-diorites) and cordilleran calc-alkaline old granites (quartz diorites, tonalites, adamellite, granodiorites), Dokhan volcanics, Hammamat sediments, felsite porphyry, Feirani volcanics, younger granite (monzogranites, syenogranites and alkali-feldspar granites), rift related riebeckite granite, dikes and quartz veins.

The Older Syn-Orogenic Granites comprise gabbro-diorite, tonalite, trondhjemite and granodiorite intrusions of emplacement between 700 and 750 Ma [10] and between 830 and 978 Ma by Rb/Sr method. These granites were followed by late- to post-tectonic (650-520 Ma) younger group of granodiorites, granites and alkali feldspar granites [11, 12, 13, 14, 15, 16, 17, 18 & 19].

The Y Gr of El-Urf, El-Dob and Abu-Kharif bodies are located within the Northern tectonic domain between latitudes 26° 37′ and 26° 50′ N and longitudes 33° 20′ and 33° 28′ E (Fig. 1a). These three Y Gr bodies constitute with El-Erediya, El-Gidami, Ria El-Garrah and El-Misskat the Western Arch (WA, Fig. 1b) recognized by [20].

The three studied granite bodies are differentiated by [8] into three main phases buff biotite-hornblende granite, pink perthitic leucogranite and yellowish pink riebeckite granite. As well, El-Urf granite is considered syenogranite [24 & 25], while El-Dob is leucocratic biotite granite [26], and Abu-Kharif alkali feldspar granites [27].

The WA Y Gr is dissected by Safage-Qena tectonic discontinuity into two geochemical provinces; El-Missikat El-Erediya to the South and El-Urf Abu-Kharif in the North. El-Erediya - El-Missikat considered geochemical province is bearing Mo porphyry- U in El-Erediya El-Missikat , F - U deposits in El Gdami – Ria El-Garrah, W-Mo-Pb-Zn-Cu bearing greisen zones and polymetallic veins in El-Missikat [20]. Northwards, El-Urf - Abu-Kharif geochemical province is bearing two types of mineralization U in El-Urf and Mo-W in El-Dob and W in Abu-Kharif. Similarly, Umm El Huwitat-Abu Hawies Y Gr bodies constitute the Eastern arch recognized by [20]. Both arches are surrounding from south to north Meatiq Ophiolite Group, Island arc rock unites and Older Syn-orogenic granite extending (150km) forming a large belt trending NW [20]. As a result; these granite bodies of both arches represent this stage.

A change in the tectonic regime from compression to extension is associated with U-F-Au deposits in the Eastern Desert. These deposits occurred at the end of a super-continental cycle that characterized by subduction related granitoid magmatic hydrothermal heated fluid in the core of hydrothermal system precipitated the main U deposits, and also rushed water and minerals towards the upper continental rocks. The water that was filtering these rocks came from the Mozambique Ocean when subduction occurred that deposited the U silicate minerals, (uranophene, beta-uranophene, kasolite) and other associated deposits in upper level of the continental crust.

The aim of the study is an approach to recognize geochemical pathfinders and genesis of such mineralization using remote sensing techniques and field study, alteration processes, geochemical behavior of elements and elemental ratios.

2. MATERIALS AND METHODS

Integration of fieldwork, Landsat-8 & ASTER data analysis and [21] were used to recognize the rock types , alterations types, and structural elements (lineaments, faults, shear zones) verified by field study and to determine the exposed rock types , lineaments, structures and alterations. The applied remote sensing-based analysis are Landsat-8 (scene path 174, row 42) acquired on June 24, 2021 and ASTER Level-1B, date November 11, 2005 with radiometric and geometric correction coefficients, projected to UTM, Zone 36 North and datum WGS-84. Digital image processing was also applied using ENVI 5.2, and Arc GIS (10.3) Software programs. The processing methods include false color composite (FCC), band ratio (BR) and principal component analysis (PCA).

The Principal Component Analysis (PCA) using [28] technique, determined the best four bands for each alteration mineral: two for maximum reflectance and the other two for absorption features. According to the alteration products found in the study area through field, petrographic and previous works, the following common end member alteration minerals were selected: sericite, illite, chlorite and hematite.

Fifteen of the collected samples were subjected to X-ray fluorescence analysis to determine the content of major oxides and trace elements. The applied instrument is the Axios Sequential apparatus WD XRF Spectometer, Philips- P Analitical 2005, the ASTM E1621 standard guide for elements analysis by wavelength dispersive X-ray fluorescence spectrometer and ASTM D7348 standard test method for Loss on Ignition (L.O.I.) of solid combustion were used as guideline of the Model at the laboratories of the National Research Center, Gizza, Egypt. The author estimated Loss on Ignition (L.O.I.) by ignition of each weighed sample using muffle furnace for sixty minutes at 1000° C at the Geochemical Lab., Department of Geology, Faculty of science, Al Azhar University, Cairo branch.

Processing and graphing the contents of the major oxides (MgO, CaO, Fe_2O_3, K_2O, and Na_2O) and trace elements (Ga, Zn, Ni, Cu, Rb, Sr, Y, and Zr), elemental ratios and the correlation coefficient (r) values. Besides, such data given in previous studies are also used to gain values of elements Clark of concentration (CC), binary relationships of elements to detect the geochemical characteristics, magma type and tectonic setting of the three bodies.

3. GEOLOGIC SETTING

The studied El-Urf Abu-Kharief area is covered by Amphibolite schist, island arc metavolcanics, Older Syn-orogenic Granites and late to post magmatism (gabbro and Younger Late-Orogenic Granites) mostly invaded by post tectonic swarms of dykes and veins (Fig. 1). The metavolcanic rocks occupy the western part of the mapped area and represented by metabasalt and metaandesite.

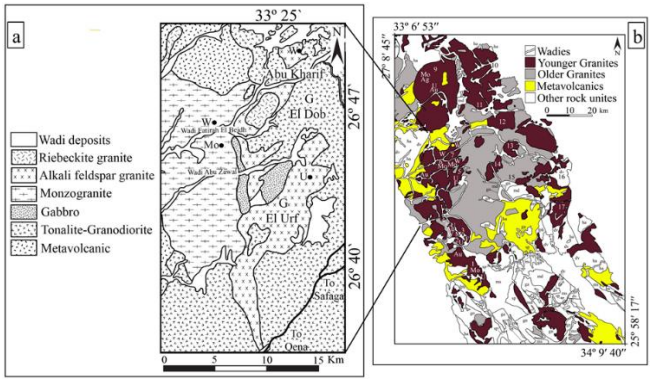

Fig. 1: (**a**) the geologic map of El-Urf, El-Dob and Abu-Kharif Y Gr outcrops, after [21], modified after [22]. (**b**) The granitic outcrops of the two convex arches modified after [23] are (1) G. El-Eradiya, (2) G. El-Gidami, (3) G. Ria El- Garrah, (4) G. El-Missikat, (5) G. El Urf, (6) G. El Dob, (7) W. El Dob, (8) G. Abu Kharif, (9) G. Qattar, (10) W. Faliq el-Wair, (11) G. Shayib, (12) G. Umm Anab, (13) G. Ras Barud, (14) G. Abu Hawis, (15) G. Abu Furad, (16) G. Nuqqara, (17) G. Umm-El Huwitat, . Gabbro (ga), Post-Hammamat Felsite (fph), Hammamat group (ha), Dokhan Volcanics (dv), Metagabbro-Diorite complex (md), Serpentinite (sp), Metasediments (ms), and Paragneisses and Migmatites (gn).

The Older Syn-Orogenic granites extending farther to the east comprise tonalite-granodiorite rocks. They are medium to coarse - grained

greyish rocks, with predominant xenoliths and alignment of mafic minerals in the form of gneissose texture. They are highly jointed and cross-cut by the (biotite-hornblende granite) monzogranite, as well as the perthitic leucogranite (alkali feldspar granite) of Gebel El-Urf (Fig. 2a).

Gabbro (dark greyish, massive, with low-moderate relief) is located at the west of Gebel El-Urf and invaded with sharp contacts by younger Late-Orogenic granites.

The Younger Late-Orogenic granites are represented by monzogranite, syeno- and alkali feldspar granite. Monzogranite forms low lands, jointed, and shows weathered exfoliation. They have many xenoliths and cut by numerous NE dykes and faults (Fig. 2b, c).

The alkali feldspar granite is often massive and devoid nearly of dykes as compared with the monzogranite. The pegmatite and quartz veins are often associated with it particularly along their fractures and joints (Fig. 2d, e, f).

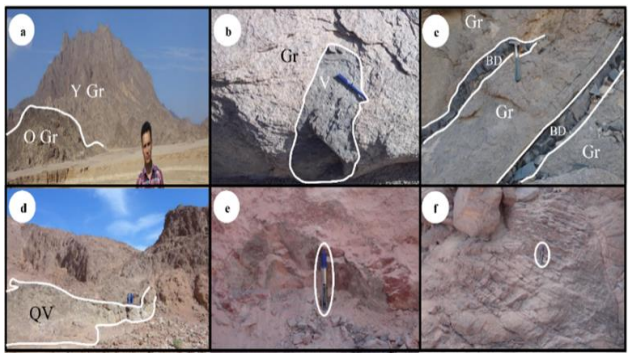

Fig. 2: Field photographs show (**a**) Older Syn-Orogenic (O Gr) and Younger Late-Orogenic (Y Gr) granites, looking (E); (**b**) Xenolith of volcanic rock (V) in granite (Gr), looking (N); (**c**) Basic dyke (BD) cutting granite (Gr), looking (N); (**d**) Quartz vein, looking (EW) ; (**e**) Mineralized pegmatite pocket, looking (E) (**f**) Fractured granite, looking (E).

The alkali feldspar granites form an elongated high relief NE belt extending from Gebel El-Urf to Gebel El-Dob (Fig. 3). They are medium-grained, pink to red color and composed essentially of K-feldspars, quartz and minor plagioclase.

These rock types are distinguished using the false-color composite FCC into Y. Gr. in light blue color, O. Gr. in pale violet and Gabbroic rock in dark brown (Fig. 3).

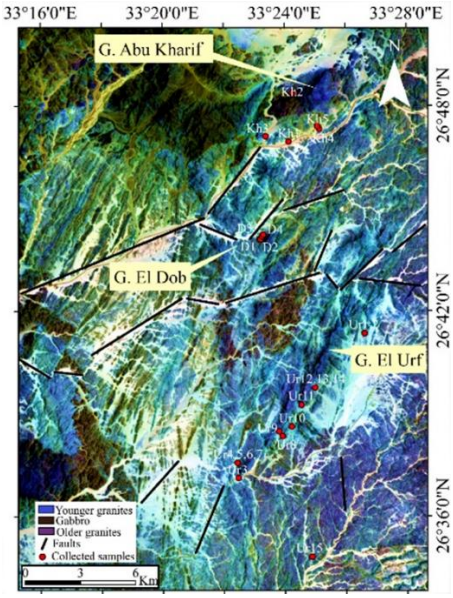

Fig. 3: Landsat-8 false colour composite (FCC) image of 2, 4, 7 in RGB discriminating Older Syn-Orogenic and Younger Late-Orogenic Granites and showing the extracted faults and collected samples.

The obtained lineament maps output of automatic lineament extraction using the Line Module in PCI Geomantic software shows that the three studied granite bodies subjected to intense deformation processes. The rose diagrams are generated using the rockworks15 software for the lineaments for each of the three granite bodies show probable trend. The chief of El-Urf granite is NE and NNE similar to El-Missikat pluton recognized by [20], El-Dob granite lineaments poses WNW and NNW, while Abu-Kharif lineaments trend is NNE (Fig. 4).

The detected alterations using band ratio and the principal component analysis (PCA) are thepropylitic, phyllic and argillic types. In this respect, such propylitic alteration type occurred in granite as mentioned by [29]. The band ratios (4/2-4/5-5/6) of [30] in RGB detected the propylitic (250-400°C) alteration type (Fig. 5). The phyllic (200- 450°C) and argillic (100-300°C) alterations are detected using the Aster 4/6 and 4/ (5+6) band ratios, respectively [31]. The argillic and phyllic types are strongly affected El-Urf, El-Dob and Abu-Kharif areas. While the propylitic type is detected in small scale at only El-Urf and El-Dob. Sericite-illite, chlorite, and hematite are the detected alteration minerals (Fig. 6) using the technique given by [28].

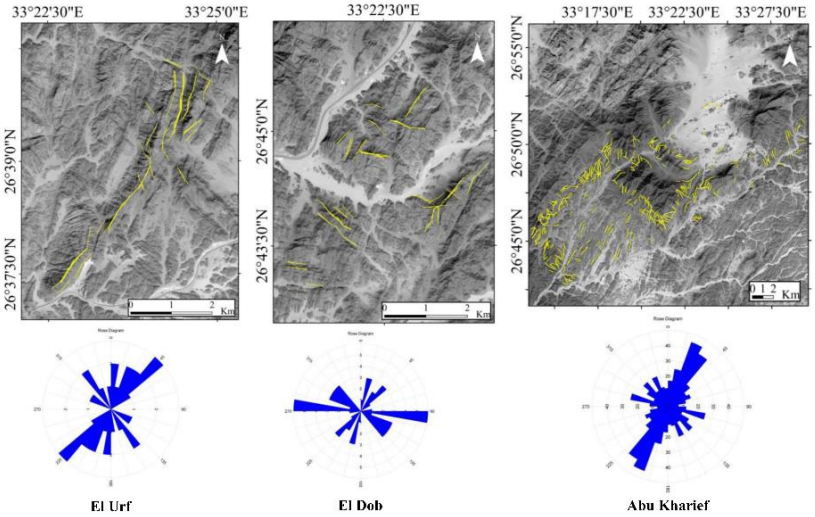

Fig. 4: Lineaments of the studied granites outcrops with rose diagrams.

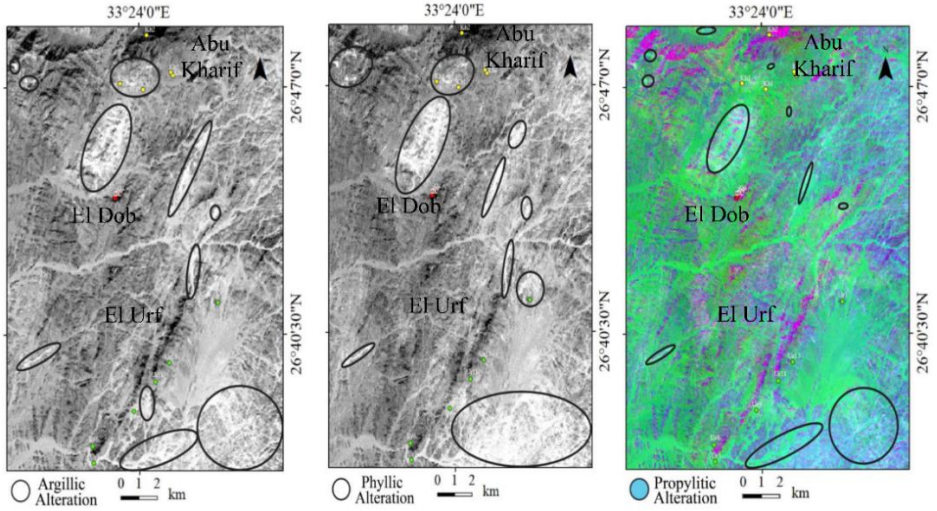

Fig. 5: Aster 4/ (5+6) of [31], (4/2-4/5-5/6) of [30] and 4/6 of [31] band ratios showing the argillic, propylitic and phyllic alteration types.

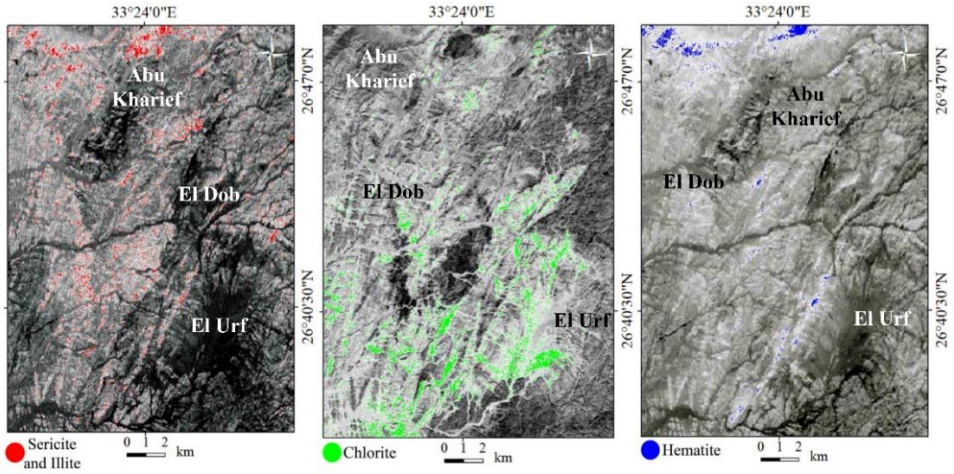

Fig. 6: Aster PC3 image showing sericite-lllite, chlorite and hematite alteration minerals.

4. RESULTS

4.1. Geochemical Characterization

The plotted geochemical binary relationships of Fe_2O_3 VS MgO following [20] discriminate the studied granites into monzo-, syeno- and alkali feldspar granites. The obtained results are supported by K/ Na ratio <1, >1 < 1.6, and >1.6 (Table 1) respectively. These characterise the geochemical dispersion of these oxides of each diagram. The Fe_2O_3 VS Mg O for the analysed fifteen samples show that four samples of only El-Dob and Abu-Kharif deviated from the dividing line of [20] reflecting ferrugenation for both granites (Fig. 7).

Table 1: K/Na values of the studied Y Gr samples

S. No.	Field No.	Area	K/Na
1	Ur1	El-Urf	1.337
2	Ur3		1.238
3	Ur6		0.98
4	Ur9		1.271
5	Ur11		0.96
6	Ur13		1.198
7	D1	El-Dob	0.947
8	D2		1.724
9	D3		1.707
10	D4		1.84
11	Kh1	Abu-Kharif	1.058
12	Kh2		1.364
13	Kh3		1.222
14	Kh4		1.307
15	Kh5		1.135

The major oxides of the fifteen chemical analyses (Table 2) plotted on binary geochemical relationships indicate the following characteristics:-

- Na_2O+K_2O VS SiO_2 variation diagrams of [32] (Fig. 8 a) and [33] (Fig. 8 b) recognize the three studied granites plotting in the field of alkali granite and in both fields of granite and alkali feldspar granite respectively due to effect of alteration process.

- On the $(Al_2O_3 + CaO)$ / $(FeOt + Na_2O + K_2O)$ VS 100 $(MgO + FeOt + TiO_2)$/ SiO_2 diagram of [34] (Fig. 9 a) point that the plotted samples represent highly fractionated calc-alkaline granite to calc-alkaline granite.

- The plotted binary diagrams of Rb VS Nb+Y of [35 & 36] (Fig. 9 b) express that these granites belong to post-collision, volcanic arc and within plate granite tectonic regime.

4.2. Geochemical distribution of Trace Elements

The calculated Clarke of concentration (CC) for the trace elements in the studied samples (Table 3) relative to their average contents of low calcium granite of [37], correlation coefficient (r) of Ga, Zr, Ba, Rb, Sr, Cr, Nb, Y, Zn, Cu, Ni and the plotted binary relationships of both Ga, Zn, Ni, Rb and Sr VS Fe2O3 and Cu, Zn, Ni, Y VS Ga exhibit the following characteristics: -

a- The Clark of concentration values (CC) show that the lithophile elements Rb, Zr, Y, Ba, and Nb possess normal distribution for the studied bodies, except Nb and Zr in two sample from El-Dob possess abnormal anomalous concentration (Nb CC- 3, and Zr CC- 7), and one sample from Abu-Kharif granites (Nb CC- 6, Zr CC- 6)

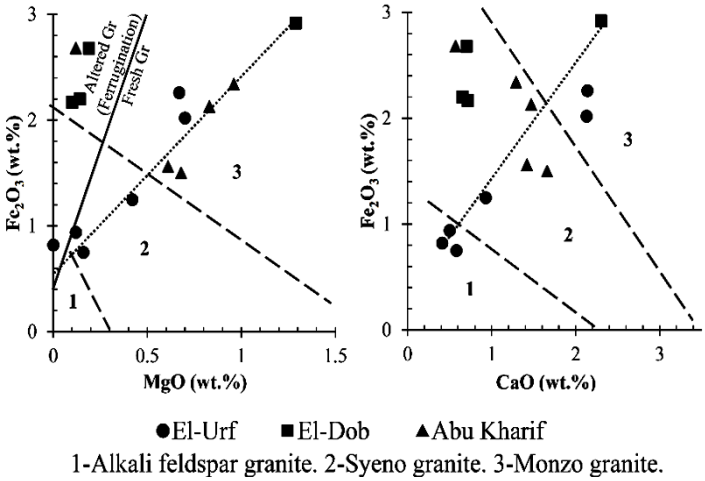

Fig. 7: Plots of the studied granites on Fe_2O_3 vs. MgO and Fe_2O_3 vs. CaO binary relationships, the plotted lines are given by [20].

b- The Clark of concentration values (CC) of only Ni, Cu, Zn and Ga chalcophile elements possess abnormal anomalous concentration in three samples of El-Urf body (Ni CC 18, 18, 13, Cu 3, 4, 6 and Zn CC 3) and in two samples of El-Dob (Ni CC 9, 9, Cu 5, 6 Zn 4, 5, and Ga CC-3), and in two samples of Abu-Kharif granite (Ni CC 9, 11, Cu 3, 4, Zn 4, 4). The extraordinary concentration of Ni and abnormal concentration of Cu and Zn point to probable presence of sulphide minerals within their NE trending greisen zones matching with El-Missikat greisen zone bearing the proper minerals W, Mo, Cu, Zn and Pb within the shear zone trending NE. These results point to the role of the structures as a controlling factor of localization and the magmatic hydrothermal origin of both types of the mineralization.

c- Also interesting notice Ti vice versa Cr record highly anomalous contents in the three granite bodies. Also, Both Cr and Ni show highly anomalous contents in most samples.

d- The three studied bodies similar to the southern four bodies of the Western arch [20] exhibit anomalous concentration of Cr (18-3 CC values), Zn in only El-Dob and Cu (CC-6-4) except one sample of El-Dob and two of Abu-Kharif.

e- Most of the samples record extraordinary anomalous concentrations of Ni as CC values are ranging from 18-5.

f- Abnormal anomalous concentration of Ga, Zn, and Nb are recorded in some samples of El-Dob and Abu-Kharif granites. On other hand Ba shows lower concentration in some of the samples.

The plotted binary relationships of each of Cu, Zn, Ni, Ga, Rb and Sr VS Fe_2O_3 (Fig. 10) and also VS Ga (Fig. 11) recognize positive

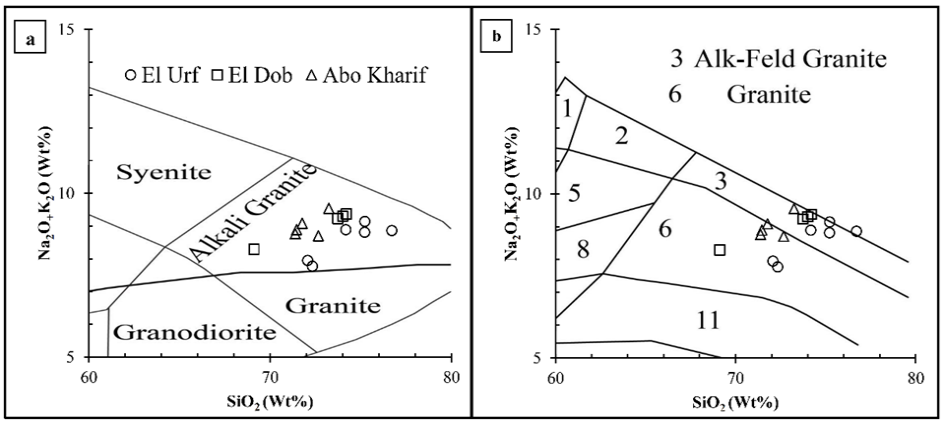

Fig. 8: a) The SiO_2 vs. Na_2O+K_2O variation diagram for the studied granitic rocks of [32], and **b**) [33].

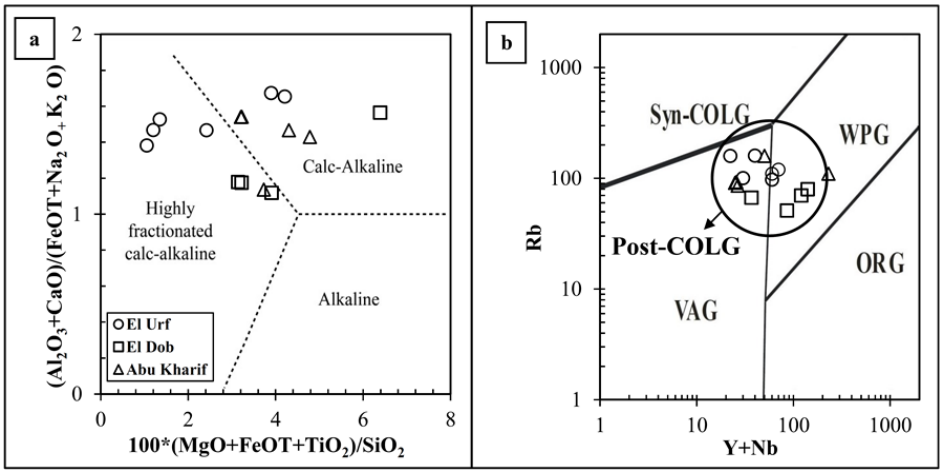

Fig. 9: Plots of the granitic samples on **a**) [34] binary diagram, **b**) Rb vs. Nb+Y binary diagram of [35, 36], WPG, within-plate granite; ORG, ocean-ridge granite; VAG, volcanic-arc granite; syn- COLG, syn-collision granite, post- COLG, post -collision granite.

correlation patterns for Zn, and Sr VS Fe_2O_3 and each of Cu, Zn, Ni, Y VS Ga and negative correlation patterns for each of Ga, Ni, Rb VS Fe_2O_3. This geochemically favours presence of Cu, Zn, and Ni in the form of sulphide minerals similar to that recorded in El-Missikat [20] associating with the W-Mo mineral deposits. Meanwhile, the positive correlation pattern of Y VS Ga recognizes its presence encountered within the crystal lattice of the silicate minerals.

The binary correlation patterns of Na_2O VS K_2O, Fe_2O_3 VS CaO, Zn VS Cu, Sr VS Rb, eU VS K, Zr VS K using the chemical analyses of the studied granites from previous studies recorded positive correlation patterns of Fe_2O_3 VS CaO and Cu VS Zn for the three bodies and K_2O VS Na_2O for El-Urf, but negative correlation pattern for El-Dob (Fig. 12).

Table 2: Major oxides (wt. %) and trace elements (ppm) of the studied samples

Area	El Urf						El Dob				Abo Kharif					Low calcium granite*
S. No.	Ur1	Ur3	Ur6	Ur9	Ur11	Ur13	D1	D2	D3	D4	Kh1	Kh2	Kh3	Kh4	Kh5	
Major oxides																
SiO_2	72.33	74.17	75.21	75.22	76.71	72.07	69.11	74	74.2	73.73	71.46	73.24	71.77	71.38	72.66	74.25
TiO_2	0.34	0.25	0.05	0.07	0.07	0.29	0.5	0.27	0.27	0.28	0.33	0.20	0.30	0.35	0.30	0.19
Al_2O_3	14.08	13.76	14.25	13.83	12.86	14.22	14.78	12.56	12.69	12.33	14.38	13.02	14.74	14.24	13.83	13.5
Fe_2O_3	2.26	1.25	0.94	0.75	0.82	2.02	2.92	2.17	2.20	2.68	2.13	2.68	1.56	2.34	1.50	2.03
CaO	2.14	0.93	0.50	0.58	0.41	2.13	2.30	0.71	0.65	0.70	1.47	0.57	1.42	1.29	1.66	0.6
MnO	0.05	0.03	0.02	0.06	0.04	0.07	0.12	0.05	0.06	0.12	0.09	0.05	0.05	0.10	0.06	0.04
MgO	0.67	0.42	0.12	0.16	0.00	0.70	1.29	0.10	0.14	0.19	0.83	0.12	0.61	0.96	0.68	0.26
Na_2O	3.54	4.22	4.69	4.28	4.77	3.84	4.49	3.66	3.71	3.49	4.57	4.30	4.34	4.04	4.32	3.4
K_2O	4.23	4.67	4.12	4.86	4.09	4.11	3.80	5.64	5.66	5.74	4.32	5.24	4.74	4.72	4.38	5.04
P_2O_5	0.16	0.05	0.01	0.03	0.01	0.14	0.30	0.03	0.03	0.05	0.13	0.02	0.12	0.16	0.15	0.36
SO_3	0.01	0.07	0.03	0.03	0.10	0.26	0.12	0.56	0.15	0.43	0.06	0.08	0.03	0.17	0.21	-
L. O. I.	0.03	0.03	0.02	0.03	0.03	0.02	0.04	0.02	0.03	0.01	0.01	0.03	0.04	1.44	0.11	0.33
Total	99.85	99.85	99.96	100.44	99.91	99.86	99.14	99.77	99.78	99.75	99.78	99.55	99.72	101.19	99.86	100
Trace elements																
Cr	70	24	74	42.9	10.2	16.7	7	17.8	50	16.5	4.8	70	8.5	16.7	5.2	4.1
Ni	80	20	60	0.7	1.1	80	4.1	40	40	1.4	2.1	40	50	2.3	2.2	4.5
Cu	40	30	30	4.2	4.5	60	4.9	50	60	4.7	5.2	40	30	5.6	4.5	10
Zn	60	60	120	24.6	31.7	60	59	150	210	144.3	44.1	150	140	43.7	37.7	39
Zr	300	310	100	67.4	83.6	280	204.5	1160	1300	647.4	139	1090	250	135	121	175
Rb	120	110	160	100.7	97.7	150	67	70	80	51.2	91.2	110	160	85.7	92.9	170
Y	50	30	10	9.1	11.3	40	19.3	60	70	56.5	11.8	110	30	12.2	11.4	40
Ba	520	570	160	5.7	8	350	408.4	90	90	66.1	325.4	130	460	295.8	275.3	840
Sr	230	160	30	10	8.3	180	284.5	40	30	13.9	228.5	20	320	199.9	193.6	100
Ga	30	30	40	17.3	16.5	20	19.2	50	30	26.3	17.9	60	30	18.1	18	17
Nb	20	30	30	13.1	18.8	20	17.5	60	70	29.3	13.1	120	20	14.2	14.3	21
Ti	Bdl	Bdl	Bdl	117.8	137.9	Bdl	968.6	Bdl	Bdl	452.4	609.4	Bdl	Bdl	622.9	509.7	-

Bld-Below detection limit
* [37]

Table 3: Clark of concentration (CC) of the studied samples

S. No.	Field No.	Area	Ga	Zr	Ba	Nb	Rb	Sr	Y	Zn	Cr	Cu	Ti	Ni
1	Ur1	El-Urf	2	2	0.6	1	0.7	2	1	2	17	4	0	18
2	Ur3		2	2	0.7	1	0.7	2	1	2	6	3	0	4
3	Ur6		2	0.6	0.2	1	0.9	0.3	0.3	3	18	3	0	13
4	Ur9		1	0.4	0.01	0.6	0.6	0.1	0.2	0.6	11	0.4	51	0.2
5	Ur11		1	0.5	0.01	0.9	0.6	0.1	0.3	1	3	0.5	60	0.2
6	Ur13		1	2	0.4	1	0.9	2	1	2	4	6	0	18
7	D1	El -Dob	1	1	0.5	1	0.4	3	0.5	2	2	0.5	421	1
8	D2		3	7	0.1	3	0.4	0.4	2	4	4	5	0	9
9	D3		2	7	0.1	3	0.5	0.3	2	5	12	6	0	9
10	D4		2	4	0.1	1.4	0.3	0.1	1	4	4	0.5	197	0.3
11	Kh1	Abu-Kharif	1	0.8	0.4	0.6	0.5	2	0.3	1	1	0.5	265	0.5
12	Kh2		4	6	0.2	6	0.7	0.2	3	4	17	4	0	9
13	Kh3		2	1	0.6	1	0.9	3	1	4	2	3	0	11
14	Kh4		1	0.8	0.4	0.7	0.5	2	0.3	1	4	0.6	271	0.5
15	Kh5		1	0.7	0.3	0.7	0.6	2	0.3	1	1	0.5	222	0.5

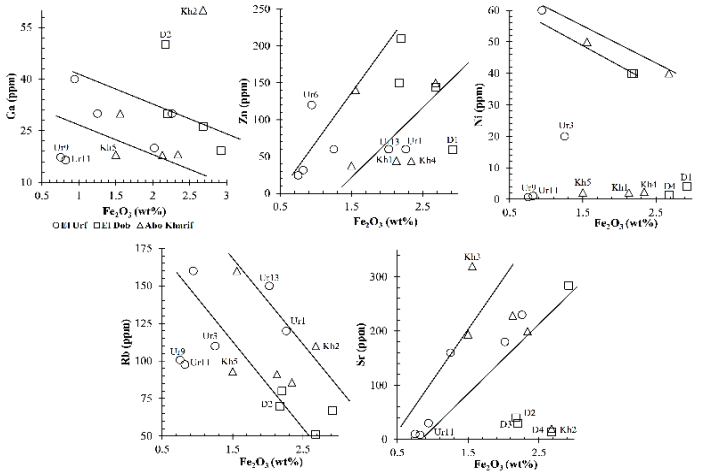

Fig. 10: The plotted binary relationships of the chalcophile Ga, Zn, Ni and lithophile Rb, Sr elements VS Fe_2O_3 of the studied samples.

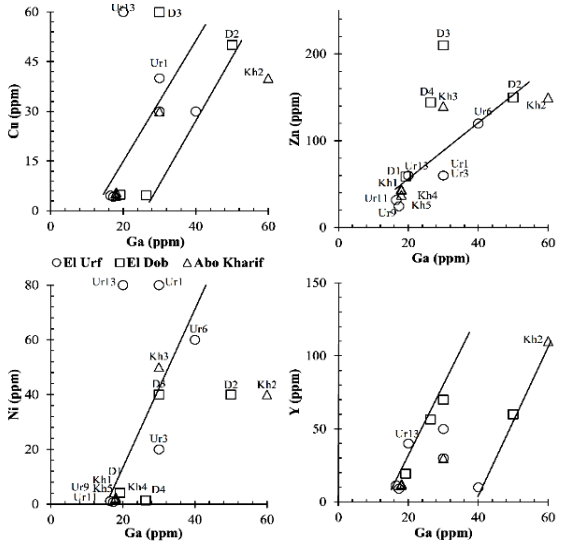

Fig. 11: Plots of binary relationships of the chalcophile Cu, Zn, Ni and Nb, Y elements VS Ga of the studied samples.

In consequence, these recorded positive correlation pattern of Na_2O VS K_2O and Fe_2O_3 VS CaO and the negative correlation pattern of Sr VS Rb are proposed to be pathfinders for revealing another W and Mo Y Gr geochemical provinces.

5. GENESIS OF MINERALIZATION

The uranium minerals are disseminated in El-Urf granite, meanwhile tungsten-molybdenum in El-Dob and tungsten in Abu-Kharif bodies are occurring as pockets in quartz veins and pegmatite trending NE are associated with the greisen-style alterations. The remote sensing PCA recognized the alteration mineral chlorite, illite and sericite in the three bodies, also slight hematite is recognized in the El-Urf and El-Dob bodies, while high hematite are revealed in the Abu Kharif Younger Late-orogenic granite.

The uranium mineralization of El-Urf granite is considered related to the genesis of El-Erediya El-Missikat uranium Molybdenum porphyry deposits. The formation of These deposits involved input in large chamber magma pulses were a magmatic hydrothermal fluid in the core of hydrothermal system and convecting heated rushed Mozambique oceanic water transported the ore metals in the outer alteration zone of the upper crust [29]. These magmatic hydrothermal fluids created formation of the El-Erediya uranium molybdenum porphyry deposits, while the U-F deposits in each of El-Gidami, Ria El-Garrah, El-Missikat and El-Urf uranium disseminated minerals are formed by convecting heated rushed Mozambique oceanic water. The mineralization changes over time from uranium molybdenum porphyry in El-Erediya central mass to El-Missikat F-U, molybdenum, wolframite hosting greisen, and polymetallic veins with sulfide gold mineralization within the sheared zone trending NE. Furthermore, uranium in El-Urf granite is followed by tungsten-molybdenum and tungsten in El-Dob Abu-Kharif respectively till the uranium deposits and Molybdnite deposit of El-Gattar. Another input of magma pulse happened that formed Mo-W greisen zone and Cu-Zn sulfide-gold mineralizations of El-Missikat and Mo-W and W of El-Dob and Abu- Kharif Late-orogenic Granite bodies.

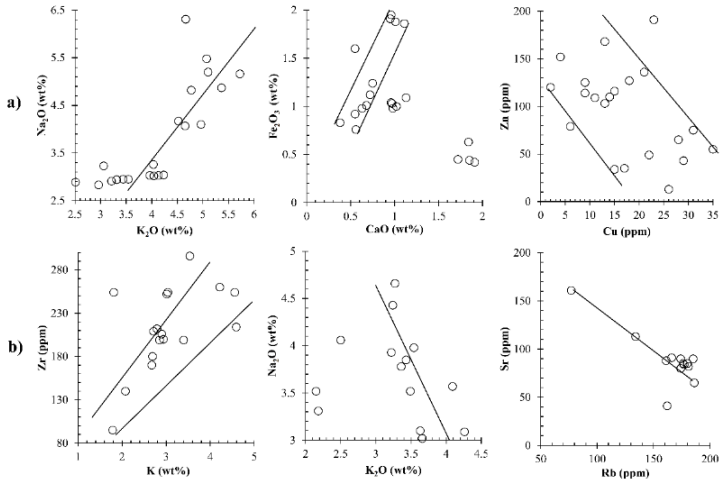

Fig. 12: Plots of binary relationships from previous chemical analyses, **a)** El-Urf granite of [8] and **b)** El-Dob-Abo Kharif granite of [26].

6. CONCLUSIONS

1-The studied granites are geochemically altered monzo-, syeno- and alkali feldspar with advanced differentiated calc-alkaline affinity and were formed in active continental margin. They are altered by propylitic, phyllic, and argillic processes, forming a distinct geochemical province of U-Mo-W hydrothermal mineral deposits.

2-The studied Y Gr and other rock types are distinguished. The extracted lineaments show variable trends: El-Urf Y Gr-NE and NNE similar to El-Missikat pluton, El-Dob Y Gr-WNW and NNW while Abu-Kharif is NNE.

3-The Clark of concentration values (CC) show that the lithophile elements Rb, Zr, Y, Ba, and Nb possess normal distribution for the studied bodies, except Nb and Zr in two sample from El-Dob possess abnormal anomalous concentration and one sample from Abu-Kharif granites. Meanwhile, the Clark of concentration values (CC) of only Ni, Cu, Zn and Ga chalcophile elements possess abnormal anomalous concentration in three samples of El-Urf body, two samples of El-Dob, and two samples of Abu-Kharif granite.

4-The positive correlation patterns of Zr VS K and negative of Na_2O VS K_2O and Sr VS Rb are characteristic geochemical pathfinders for such W-Mo mineralized province that can be used to explore other mineralised Syn-Orogenic Granites.

5- El-Dob and Abu-Kharif Y Gr bodies constitute W-Mo geochemical province. The uranium minerals are disseminated in El-Urf granite, meanwhile tungsten-molybdenum in El-Dob and tungsten in Abu-Kharif bodies are occurring as pockets in quartz veins and pegmatite trending NE are associated with the greisen-style alterations. Another input of magma pulse happened that formed Mo-W greisen zone and Cu-Zn sulfide-gold mineralization of El-Missikat and Mo-W and W of El-Dob and Abu- Kharif Late-orogenic Granite bodies.

REFERENCES

[1] Kröner A, Todt W, Hussein IM, Mansour M, Rashwan AA. Dating of late Proterozoic ophiolites in Egypt and Sudan using the single grain zircon evaporation technique. Precambrian Research. 1992; 59: 15-32.

[2] Stern RJ, Gottfried DG, Hedge CE. Late Precambrian rifting and crustal evolution in the northeastern Desert of Egypt. Geology. 1984; 12: 168-172.

[3] Stern RJ. Arc assembly and continental collision in the Neoproterozoic East African Orogen: Implications for the consolidation of Gondwanaland. Ann Rev Earth Planet Sci. 1994; 22: 319-351.

[4] Jacobs J, Thomas RJ. Himalayan-type indenter-escape tectonicsmodel for the southern part of the late Neoproterozoic-early Paleozoic East African-Antarctic Orogen. Geology. 2004; 32:721-724.

[5] EI Gaby S, List FK, Tehrani R. Geology, evolution and metallogenesis of the Pan-African Belt in Egypt. In: EI-Gaby, S., Gre iling, R.O. (Eds.), The Pan-African Belt of Northeast Africa and Adjacent Areas. Friedrich Vieweg und Sohn, Braunschweig - Wiesbaden. 1988; 17-68.

[6] Hassaan MM, Al-Amin H, Al-Badry O, Hamza A, Al-Bassiouny AS. Primary survey for tungsten minerals in Abu-Kharif area, Eastern Desert, Egypt. Asw. Sci. Tech. Bull. 1980; 2: 2.

[7] Hassaan MM. Metallic Ore Deposits in the Nubian Shield in Egypt: Tectonic Environs, Geochemical Behaviour, Promising Sites. LAMBERT, Acad. Publ., London, UK. 2011; 256.

[8] Abdel Ghani IM. Geology, petrology and radioactivity of Gebel El-Urf area, Central Eastern desert, Egypt. Unpublished Ph. D. thesis, Faculty of Science, South Valley University. 2000.

[9] Tawadros E. Geology of North Africa, CRC Press. 2011; 390.

[10] Dixon TH. The evolution of continental crust in the late Precambrian Egyptian Shield. Ph D thesis, Univ Calif, San Diego. 1979.

[11] El-Ramly MF. A new geological map for the basement rocks in the Eastern Desert of Egypt; scale 1:1000, 000. Ann. Geol. Surv. Egypt. 1972; 2: 1-18.

[12] El-Gaby S. Petrochemistry of some granites from Egypt. N. Jb. Mineral. Abh. 1975; 124: 147-189.

[13] Hashad AH. Present status of geochronological data on the Egyptian basement complex. Instit. Appl. Geol. Bull., Jeddah. 1980; 4: 31-46.

[14] Rogers JJW, Greenberg JK. Trace elements in continental margin magmatism; Part III alkali granites and their relationship to cratonization. Geol. Soc. Amer. Bull. 1981; 92: 6-9.

[15] Stern RJ, Hedge CE. Geochronological and isotopic constraints on Late Precambrian crustal evolution in the Eastern Desert of Egypt. Am. J. Sci. 1985; 285: 97-127.

[16] Bentor YK. The crustal evolution of the Arabo-Nubian Massif, with special reference to Sinai Peninsula. Prcambr. Res. 1985; 28: 1-74.

[17] Stern RJ, Gottfried D. Petrogenesis of late Precambrian (575-600 Ma) bimodal suite in northeast Africa. Contributions to Mineralogy and Petrology. 1986; 92: 492-501.

[18] Hussein AA, Ali MM, El-Ramly MF. A proposed new classification of the granites of Egypt. Jour. Volcano. Geotherm. Resear. 1982; 14: 187-198.

[19] Hassan MA, Hashad AA. Precambrian of Egypt. 201-245 in: The Geology of Egypt (Said, R., Ed.). Balkema, Rotterdam. 1990; 722.

[20] Hassaan MM, Sayed AO, Ahmed EK, Taher MS, Islam ME, Sayyed MI, Hanfi MY. Prognostic Exploration of U-F-Au-Mo-W Younger Granites for Geochemical Pathfinders, Genetic Affiliations and Tectonic Setting in El-Erediya-El-Missikat Province, Eastern Desert, Egypt. Minerals. 2022; 12:518.

[21] Egyptian Geological Survey and Mining Authority (EGSMA). Geologic map of Al Qusayr Quadrangle, Egypt. Scale 1:250,000. 1992; Sheet NG 36 K.

[22] Shahin TM. Geology, geochemistry and petrotectonicof the basement rocks at Gebel El Dob area, North Eastern desert, Egypt. Unpublished Ph. D. thesis, Faculty of Science, Al-Azhar University. 2015.

[23] Egyptian Geological Survey and Mining Authority. Metallogenic Map of Qena Quadrangle, Egypt; Egyptian Geological Survey and Mining Authority: Cairo, Egypt, 1984.

[24] El-Mansi MM, Dardier AM. Contribution to the geology and radioactivity of the older granitoids and Younger Granites of Gebel El-Urf- Gebel Abu Shihat area, Eastern desert, Egypt. Delta Journal of Science. 2005; 29: 1-17.

[25] Asran AM, El-Mansi MM, Ibrahim ME, Abdel Ghani IM. Pegmatites of Gebel El Urf, Central Eastern desert, Egypt. The 7th international conference on the geology of Africa. Nov. 2013; P-P IV-1- IV-22.

[26] El Sheshtawi YA, Yossef F, Ammar FA, Hassaan MM, Sakr SM. Petrography and geochemistry of some granites and their metavolcanic country rocks in Central Eastern Desert, Egypt. The proceeding of 1st Seminar of nuclear raw material and their technology, Cairo, Egypt. 1999; 1-3.

[27] Hassaan M, Yossef E, Ali M, Ammar F, El Sheshtawi Y, Sakr S. Geochemical behavior of some ore metals in the dispersion aureoles,

Central Eastern Desert, Egypt. Sedimentology of Egypt. 2000; Vol. 8. P.215-230.

[28] Crosta AP, Moore JM. Enhancement of Landsat thematic mapper imagery for residual soil mapping in SW Minais Gerais State, Brazil: a prospecting case history in Greenstone belt terrain. Proceedings of 7th ERIM Thematic Conference: Remote sensing for exploration geology. 1989; 1173-1187.

[29] Ridley J. Ore Deposit Geology; Cambridge University Press: Cambridge, UK, 2013; p. 409.

[30] Velosky JC, Stern RJ, Johnson PR. Geological control of massive sulphide mineralization in the Neoproterozoic Wadi Bidah shear zone, Southwestern Saudi Arabia, inferences from orbital remote sensing and field studies. Precambrian Research. 2003; 123 (2-4): 235-247.

[31] Nouri RJ, afari MR, Arain, M, Feizi F. Hydrothermal alteration zones identification based on remote sensing data in the Mahin Area, West of Qazvin Province, Iran. International Journal of Geological and Environmental Engineering. 2012; 6: 382-385.

[32] Middlemost EAK. Magmas and Magmatic Rocks. An Introduction to Igneous Petrology. Longman group Ltd., London, New York. 1985; 266.

[33] Cox KG, Bell JD, Pankhurst RJ. The interpretation of igneous rocks. London, Allen and Unwine. 1979; 450.

[34] Sylvster PJ. Post-collisional alkaline granites. J. Geoi. 1989; 97: 261-280.

[35] Pearce JA, Harris NBW, Tindle AG. Trace element discrimination diagrams for the tectonic interpretation of granitic rocks. *J. Petrol.* 1984, *25*, 956–983.

[36] Pearce J. Sources and settings of granitic rocks. Episodes. 1996; 19: 120-5.

[37] Turekian KK, Wedepohl KH. Distribution of the elements in some major types of the Earth's crust. Geological Society of America. Bulletin. 1961; 72: 175-192.

استكشاف جيوكيميائي لمعايير يورانيوم-موليبدنوم-تنجستن في الجرانيت الأصغر، الإقليم الجيوكيميائي العرف – الدب - أبو خريف، حزام الانقطاع التكتوني سفاجا-قنا، الصحراء الشرقية ، مصر

اسلام النجار [1]، محمود حسان [1]، طاهر شاهين [1]، سيد عمر [2]، احمد خليل [3]

1. قسم الجيولوجيا ، كلية العلوم ، جامعة الازهر ، القاهرة ، مصر
2. هيئة المواد النووية - القاهرة - مصر
3. . المركز القومي للبحوث - القاهرة – مصر

الملخص

تتواجد كتل جرانيت العرف والدب وأبو خريف الأصغر شمال نطاق سفاجا-قنا التكتوني البنائي، بين خطي عرض 26°37′ و 26°50′ شمالا، وخطي طول 33°20′ و 33°28′ شرقا. تشكل هذه الاجسام الثلاثة من الجرانيت الاصغر اقليم جيوكيميائي حيث يستضيف جرانيت العرف يورانيوم، بينما يستضيف جرانيت الدب وأبو خريف تنجستن- موليبدنوم و تنجستن على التوالي. حدد تكامل الدراسة الحقلية مع تقنيات الاستشعار من البعد والدراسات الجيوكيميائية العوامل الحاكمة والأدلة ونشأة هذه الرواسب. تم تحديد الوحدات الصخرية الجرانيت الأقدم والجابرو و الجرانيت الأصغر، التراكيب وعمليات التغاير البروبيلي والفلي والأرجلي بواسطة الدراسة الحقلية وتقنيات الاستشعار من البعد. تشير التحاليل الجيوكيميائية للصخور المضيفة انها ذات طبيعة قلوية، قل كلسية شديدة التجزئة إلى قلوية ، بيئة جرانيت ما بعد التصادم . تمايزت عينات الجرانيت مونزو سيانو و قلي الفلسبار و وتاثر الصخور لعمليات تغاير باكاسيد حديد بواسطة العلاقات الثنائية الجيوكيميائية لأكسيد الحديد الثلاثي مقابل كلا من اكاسيد الماغنيسيوم والكالسيوم. تعتبر أنماط الإرتباط الإيجابية للزركونيوم مقابل البوتاسيوم والسلبية لأكسيد الصوديوم مقابل أكسيد البوتاسيوم و الإسترنشيوم مقابل الروبيديوم ادلة جيوكيميائية للجرانيت الأصغر الحامل لمثل هذه النوعية من التمعدنات. يمثل تمعدن اليورانيوم في العرف امتدادا لرواسب اليورانيوم الفقيرة المحتوي في المسيكات حيث تكونت بواسطة السوائل الحارمائية لمركز الصهاره الاولي و اندفاع مياه محيط موزمبيق الحارمائية بفعل الصهارة فاثرت علي جرانيت العرف حيث حملت بيورانيوم منخفض التركيز. حدثت دفعات جديده من الصهارة لتتكون رواسب تنجستن- موليبدنوم و كبريتيدات النحاس و الزنك في المسيكات. امتد هذا التأثير ليكون تنجستن- موليبدنوم و تنجستن في الجرانيت الأصغر للدب وابو خريف ويحتمل تقدم اندفاع الصهارة لتتكون جرانيتات الجتار المتواجد بقمته راسب موليبدنوم.